

A two-mode squeezed light based on a double-pump phase-matching geometry

Xuan-Jian He(何烜坚), Jun Jia(贾俊), Gao-Feng Jiao(焦高锋), Li-Qing Chen(陈丽清), Chun-Hua Yuan(袁春华), Wei-Ping Zhang(张卫平)

Citation: Chin. Phys. B . 2020, 29(7): 074207 . **doi:** 10.1088/1674-1056/ab8abd
Journal homepage: http://cpb.iphy.ac.cn; http://iopscience.iop.org/cpb

What follows is a list of articles you may be interested in

Electro-optomechanical switch via tunable bistability and four-wave mixing

Kamran Ullah

Chin. Phys. B . 2019, 28(11): 114209 . **doi:** 10.1088/1674-1056/ab4580

Characterize and optimize the four-wave mixing in dual-interferometer coupled silicon microrings

Chao Wu(吴超), Yingwen Liu(刘英文), Xiaowen Gu(顾晓文), Shichuan Xue(薛诗川), Xinxin Yu(郁鑫鑫), Yuechan Kong(孔月婵), Xiaogang Qiang(强晓刚), Junjie Wu(吴俊杰), Zhihong Zhu(朱志宏), Ping Xu(徐平)

Chin. Phys. B . 2019, 28(10): 104211 . **doi:** 10.1088/1674-1056/ab3f9b

Simultaneous polarization separation and switching for 100-Gbps DP-QPSK signals in backbone networks

Yu-Long Su(苏玉龙), Huan Feng(冯欢), Hui Hu(胡辉), Wei Wang(汪伟), Tao Duan(段弢), Yi-Shan Wang(王屹山), Jin-Hai Si(司金海), Xiao-Ping Xie(谢小平), He-Ning Yang(杨合宁), Xin-Ning Huang(黄新宁)

Chin. Phys. B . 2019, 28(2): 024216 . **doi:** 10.1088/1674-1056/28/2/024216

Enhancement of multiple four-wave mixing via cascaded fibers with discrete dispersion decreasing

Jia-Bao Li(李嘉宝), Ling-Jie Kong(孔令杰), Xiao-Sheng Xiao(肖晓晟), Chang-Xi Yang(杨昌喜)

Chin. Phys. B . 2017, 26(6): 064205 . **doi:** 10.1088/1674-1056/26/6/064205

Probe gain via four-wave mixing based on spontaneously generated coherence

Hong Yang(杨红), Ting-gui Zhang(张廷桂), Yan Zhang(张岩)

Chin. Phys. B . 2017, 26(2): 024204 . **doi:** 10.1088/1674-1056/26/2/024204

A two-mode squeezed light based on a double-pump phase-matching geometry*

Xuan-Jian He(何烜竖)[1], Jun Jia(贾俊)[1], Gao-Feng Jiao(焦高锋)[1], Li-Qing Chen(陈丽清)[1,†], Chun-Hua Yuan(袁春华)[1,3,‡], and Wei-Ping Zhang(张卫平)[2,3]

[1] *State Key Laboratory of Precision Spectroscopy, Quantum Institute for Light and Atoms, Department of Physics, East China Normal University, Shanghai* 200062, *China*

[2] *School of Physics and Astronomy, and Tsung-Dao Lee Institute, Shanghai Jiao Tong University, Shanghai* 200240, *China*

[3] *Collaborative Innovation Center of Extreme Optics, Shanxi University, Taiyuan* 030006, *China*

(Received 19 January 2020; revised manuscript received 30 March 2020; accepted manuscript online 18 April 2020)

We theoretically investigate the frequency-nondegenerate and frequency degenerate squeezed lights with a four-wave mixing process (4WM) driven by two pump fields crossing at a small angle. Different from a 4WM process driven by a single pump field, the refractive index of the corresponding probe field, $n_{\rm p}$, can be converted to a value that is greater than 1 or less than 1 by an angle adjustment. In the new region with $n_{\rm p} < 1$, the bandwidth of the gain is relatively large due to the slow change in the refractive index with the two-photon detuning. In this region with an exchange of the roles of the pump and probe beams, the frequency degenerate and spatial nondegenerate twin beams can be generated, which has potential application in quantum information and quantum metrology.

Keywords: four-wave mixing, phase matching, frequency degenerate and spatial nondegenerate, metrology

PACS: 42.65.–k, 42.50.Lc, 42.65.Lm, 06.20.–f **DOI:** 10.1088/1674-1056/ab8abd

1. Introduction

Quantum enhanced metrology is the use of quantum techniques to improve measurement precision, which has been received a great deal of attention in recent years.[1–3] The Mach–Zehnder interferometer (MZI) and its variants can provide high precise measurements, based on which the gravitational waves were observed.[4,5] The sensitivity of these interferometers is limited by the vacuum quantum noise injected from the unused port. To further improve measurement sensitivity, Yurke *et al.*[6] introduced a new type of interferometer in which two four-wave mixers or parameter amplifiers (PAs) occupy the place of two linear beam splitters (BSs) in the traditional MZI. It is also called the $SU(1,1)$ interferometer because it is described by the $SU(1,1)$ group, as opposed to $SU(2)$ for BSs. Because it can be used to improve measurement accuracy, these types of interferometers have received extensive attention both experimentally[7–16] and theoretically.[17–30] Kong *et al.*[18] firstly proposed a simplified scheme of PA + BS, and it can also beat the standard quantum limit of phase-measurement sensitivity by a similar amount for the $SU(1,1)$ interferometer. The improvement comes from a result of noise reduction of the interferometer because the quantum noise of the outputs of the parametric amplifier is entangled and destructive interference at the beam splitter leads to the quantum noise cancellation. The scheme of PA + BS can reduce the difficulty of the experimental implementation. However, the scheme of PA + BS requires the two outputs of the PA to be frequency degenerate and spatial modes separation. Therefore, it is worth initiating a study on how to generate a two-mode squeezed state of frequency degenerate and spatial modes separation.

The first experimental demonstration of squeezed states of light by Slusher *et al.*[31] was based on four-wave mixing (4WM) in sodium vapor. Since then, many techniques for producing different types of squeezing have been explored, each with their own advantages and limitations for particular applications.[32] Nondegenerate 4WM in a double-Λ scheme[33] was identified as a possible scheme to generate a squeezed state or squeezed twin beams, as described in Refs. [34–41].

The generated twin beams by the 4WM process in an atomic system with higher squeezing degree were firstly realized by McCormick *et al.*[40,41] based on degenerate pump fields. A single linearly polarized pump beam is crossed at a small angle with an orthogonally polarized much weaker probe beam. The 4WM process amplifies the probe and generates a quantum-correlated conjugate beam, on the other side of the pump (at a higher frequency). In this case, a pair of photons of the (single) pump is transformed, via the 4WM process, into a photon in the probe beam and a photon in the conjugate

*Project supported by the National Natural Science Foundation of China (Grant Nos. 11974111, 11474095, 11874152, 11604069, 91536114, 11654005, and 11234003), the Fundamental Research Funds for the Central Universities, China, the Science Foundation of Shanghai, China (Grant No. 17ZR1442800), and the National Key Research and Development Program of China (Grant No. 2016YFA0302001).

†Corresponding author. E-mail: lqchen@phy.ecnu.edu.cn

‡Corresponding author. E-mail: chyuan@phy.ecnu.edu.cn

© 2020 Chinese Physical Society and IOP Publishing Ltd

beam. By modulating the involved ground (excited) state with one (two) laser beam (beams), the gain and squeezing degree can be enhanced.[42,43] The best initial results for two-mode intensity-difference squeezing at low frequencies seem to be ≈ 1.5 kHz[44] to the recently reported ≈ 700 Hz[45] or even ≈ 10 Hz.[46] The generated entanglement between the probe and conjugate beams can realize quantum imaging.[47,48] The cascaded 4WM can generate the quantum correlated triple beams[49,50] and can also be used to realized $SU(1,1)$ interferometers for highly sensitive phase measurements.[16,51] This 4WM process also supports many spatial modes, making it possible to amplify complex two-dimensional spatial patterns.[52–55]

Recently, a new 4WM process driven by two pump fields at a small angle was realized,[56] where we only demonstrated the phenomena and results, without giving detailed physical explanations. Turnbull *et al.*[57] developed a good theory to illustrate a 4WM process driven by a single pump field. In this paper, we describe the two pump field phase matching that can be established between the $n_{\rm p} > 1$ and $n_{\rm p} < 1$ by the angle adjustment, which is different from the single pump case, and describe the large bandwidth of the gain varying with the two-photon detuning. The theoretical range of phase-matching angles for achieving different regions is given.

Our paper is organized as follows. In Section 2, we describe the generation of two-mode squeezed light with two pump fields crossing at a small angle. In Section 3, the phase-matching angle range is given under the condition of two pump fields driven. In Section 4, the gain of two-mode squeezed light driven by one pump field and two degenerate pump fields is compared, and by an angle adjustment the phase matching between the $n_{\rm p} > 1$ and $n_{\rm p} < 1$ is described. Finally, we conclude with a summary of our results.

2. Theoretical model for a two-mode squeezed light

The generated frequency non-degenerate squeezed light by the 4WM process is shown in Fig. 1(a). Based on the degenerate pump fields, the twin beams with higher squeezing degree were generated,[40,41] where the phase-matching geometry is shown in Fig. 2(a). In our scheme, one unique feature of this 4WM process is that two pump fields are applied at a small and adjustable angle, where the phase-matching geometry is shown in Fig. 2(b). The approach to generate the frequency degenerate twin beams is based on the idea of inverting the configuration from Fig. 1(a) to Fig. 1(b). For the geometry of a single pump field shown in Fig. 2(a), with a simple exchange of the roles of the pump and probe beams, single-mode squeezing is generated.[58] To obtain the twin beams with the same frequency that are spatially nondegenerate, the geometry of two non-collinear pump fields shown in Fig. 2(b) is needed.

In this section, we firstly theoretically describe the frequency non-degenerate and degenerate squeezed light based on a non-collinear 4WM process. As shown in Figs. 3(a) and 3(b), the double-Λ four-level processes of frequency non-degenerate and degenerate are the same except that the magnitudes of the detunings are different. Therefore, the frequency-degenerate and non-degenerate squeezed lights based on non-collinear 4WM can be described by a same set of equations.

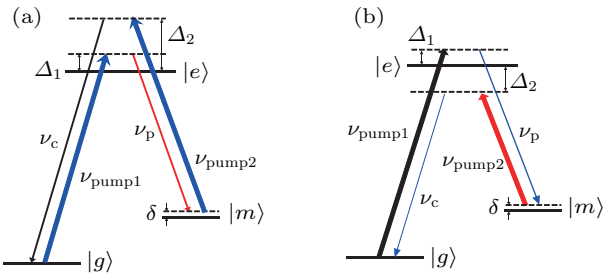


Fig. 1. Double-Λ scheme on the D_1 line of ^{85}Rb configuration for the generation of (a) the frequency non-degenerate and (b) frequency degenerate squeezed lights. The state $|g,m\rangle$ involves the hyperfine levels $|5S_{1/2},F=2,3\rangle$. The hyperfine splitting of the excited state is not resolved due to Doppler broadening.

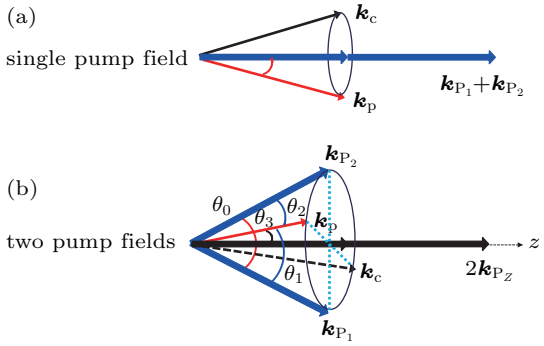


Fig. 2. The geometric phase matching for (a) a single pump field and (b) two pump fields. The angle between pump fields $\boldsymbol{k}_{\rm P_1}$ and $\boldsymbol{k}_{\rm P_2}$ is θ_0. The angles between the probe field $\boldsymbol{k}_{\rm p}$ and the pump fields $\boldsymbol{k}_{\rm P_1}$ and $\boldsymbol{k}_{\rm P_2}$ are θ_1 and θ_2, respectively. Here θ_3 is the angle between the probe and the projected pump field. The frequency degenerate twin beams are generated with an exchange of the roles of the pump and probe beams.

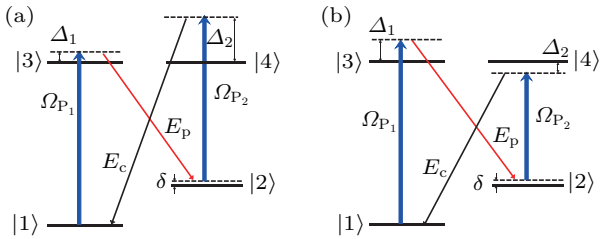


Fig. 3. (a) Double-Λ scheme with two pump fields P_1 and P_2 for (a) the frequency non-degenerate and (b) frequency degenerate squeezed lights. States $|3\rangle$ and $|4\rangle$ are orthogonal linear combinations of magnetic states of the excited hyperfine levels. $\Omega_{\rm P_1}$ and $\Omega_{\rm P_2}$ are the Rabi frequencies, Δ_1 $(=\omega_{\rm P_1}-\omega_{31})$ and Δ_2 $(=\omega_{\rm P_2}+\delta-\omega_{42})$ are the detunings, and δ is the two-photon detuning.

We assume that the two pump fields $E_{\rm P_1}$ and $E_{\rm P_2}$ couple the transitions $|1\rangle \rightarrow |3\rangle$ and $|2\rangle \rightarrow |4\rangle$, respectively. The probe field couples the transition $|2\rangle \rightarrow |3\rangle$, and the conjugate field couples the transition $|1\rangle \rightarrow |4\rangle$. The transitions $|1\rangle \rightarrow |2\rangle$ and

$|3\rangle \rightarrow |4\rangle$ are not dipole allowed transitions. In the dipole and rotating wave approximations, the Hamiltonian of the atoms combined with the Hamiltonian of the light-atom interaction is given by

$$\hat{H} = \hat{H}_{\text{atoms}} + \hat{H}_{\text{I}}, \tag{1}$$

where

$$\begin{aligned}
\hat{H}_{\text{atoms}} &= \hbar\omega_{41}\sigma_{44} + \hbar\omega_{31}\sigma_{33} + \hbar\omega_{21}\sigma_{22}, \qquad (2)\\
\hat{H}_{\text{I}} &= -\hbar(\Omega_{\text{P}_1}\,\mathrm{e}^{\mathrm{i}(\boldsymbol{k}_{\text{P}_1}\cdot\boldsymbol{r}-\omega_{\text{P}_1}t)}\sigma_{31}\\
&\quad + \Omega_{\text{P}_2}\,\mathrm{e}^{\mathrm{i}(\boldsymbol{k}_{\text{P}_2}\cdot\boldsymbol{r}-\omega_{\text{P}_2}t)}\sigma_{42} + g_{\text{p}}\hat{\mathcal{E}}_{\text{p}}\,\mathrm{e}^{\mathrm{i}(\boldsymbol{k}_{\text{p}}\cdot\boldsymbol{r}-\omega_{\text{p}}t)}\sigma_{32}\\
&\quad + g_{\text{c}}\hat{\mathcal{E}}_{\text{c}}\,\mathrm{e}^{\mathrm{i}(\boldsymbol{k}_{\text{c}}\cdot\boldsymbol{r}-\omega_{\text{c}}t)}\sigma_{41}) + \text{H.c.} \qquad (3)
\end{aligned}$$

Here $\omega_{n1} = \omega_n - \omega_1$ $(n = 2,3,4)$, $\sigma_{nm} = |n\rangle\langle m|$ $(n,m = 1,2,3,4)$, $2\Omega_{\text{P}_1} = \mu_{31}\mathcal{E}_{\text{P}_1}/\hbar$ and $2\Omega_{\text{P}_2} = \mu_{42}\mathcal{E}_{\text{P}_2}/\hbar$ are the Rabi frequencies, g_n $(n = \text{p},\text{c})$ are the atom-field coupling constants, and $\hat{\mathcal{E}}_{\text{p}}$ and $\hat{\mathcal{E}}_{\text{c}}$ are the slowly varying envelope operators of the probe and conjugate field.

The equations for the atomic operators σ_{nm} $(n,m = 1,2,3,4)$ in the Heisenberg picture are given in the Appendix. Using the atomic operators to evaluate the linear and nonlinear components of the polarization at ω_{p} and ω_{c}, the polarization of the atomic medium at a particular frequency is given by $\hat{P}(\omega_{\text{p}}) = Nd_{23}\tilde{\sigma}_{23} + \text{H.c.}$ and $\hat{P}(\omega_{\text{c}}) = Nd_{14}\tilde{\sigma}_{14} + \text{H.c.}$, where N is the number density of the atomic medium. The polarizations of the medium at frequency ω_n $(n = p,c)$ are given by

$$\begin{aligned}
\hat{P}_{\text{p}}(\omega_{\text{p}}) &= \varepsilon_0\chi_{\text{pp}}(\omega_{\text{p}})\hat{\mathcal{E}}_{\text{p}}\,\mathrm{e}^{\mathrm{i}\boldsymbol{k}_{\text{p}}\cdot\boldsymbol{r}}\\
&\quad + \varepsilon_0\chi_{\text{pc}}(\omega_{\text{p}})\hat{\mathcal{E}}_{\text{c}}^{\dagger}\,\mathrm{e}^{\mathrm{i}(\boldsymbol{k}_{\text{P}_1}+\boldsymbol{k}_{\text{P}_2}-\boldsymbol{k}_{\text{c}})\cdot\boldsymbol{r}} + \text{H.c.}, \qquad (4)\\
\hat{P}_{\text{c}}(\omega_{\text{c}}) &= \varepsilon_0\chi_{\text{cc}}(\omega_{\text{c}})\hat{\mathcal{E}}_{\text{c}}\,\mathrm{e}^{\mathrm{i}\boldsymbol{k}_{\text{c}}\cdot\boldsymbol{r}}\\
&\quad + \varepsilon_0\chi_{\text{cp}}(\omega_{\text{c}})\hat{\mathcal{E}}_{\text{p}}^{\dagger}\,\mathrm{e}^{\mathrm{i}(\boldsymbol{k}_{\text{P}_1}+\boldsymbol{k}_{\text{P}_2}-\boldsymbol{k}_{\text{p}})\cdot\boldsymbol{r}} + \text{H.c.} \qquad (5)
\end{aligned}$$

Here the two coefficients χ_{pp} and χ_{cc} describe the effective linear polarization processes for the probe and conjugate fields, respectively, and unlike the usual linear coefficients, they depend nonlinearly on the pump field. The other two coefficients χ_{pc} and χ_{cp} are responsible for the 4WM process. A detailed calculation is given in the Appendix.

Under the condition of the slowly varying amplitude approximation, considering nearly co-propagating beams along the z axis, these field equations in the co-moving frame are written as

$$\frac{\partial}{\partial z}\hat{\mathcal{E}}_{\text{p}} = \frac{\mathrm{i}k_{\text{p}}}{2}[\chi_{\text{pp}}(\omega_{\text{p}})\hat{\mathcal{E}}_{\text{p}} + \chi_{\text{pc}}(\omega_{\text{p}})\hat{\mathcal{E}}_{\text{c}}^{\dagger}\,\mathrm{e}^{\mathrm{i}\Delta k_z z}], \tag{6}$$

$$\frac{\partial}{\partial z}\hat{\mathcal{E}}_{\text{c}} = \frac{\mathrm{i}k_{\text{c}}}{2}[\chi_{\text{cc}}(\omega_{\text{c}})\hat{\mathcal{E}}_{\text{c}} + \chi_{\text{cp}}(\omega_{\text{c}})\hat{\mathcal{E}}_{\text{p}}^{\dagger}\,\mathrm{e}^{\mathrm{i}\Delta k_z z}], \tag{7}$$

where Δk_z is the projection of the geometric phase mismatch $\Delta\boldsymbol{k} = \boldsymbol{k}_{\text{P}_1} + \boldsymbol{k}_{\text{P}_2} - \boldsymbol{k}_{\text{p}} - \boldsymbol{k}_{\text{c}}$ on the z axis. The solutions to the propagation equations (6) and (7) with a medium of length L are given by

$$\hat{\mathcal{E}}_{\text{p}} = G_1\hat{\mathcal{E}}_{\text{p}}(0) + g_1\hat{\mathcal{E}}_{\text{c}}^{\dagger}(0), \tag{8}$$

$$\hat{\mathcal{E}}_{\text{c}}^{\dagger} = \left[G_2\hat{\mathcal{E}}_{\text{c}}^{\dagger}(0) + g_2\hat{\mathcal{E}}_{\text{p}}(0)\right]\mathrm{e}^{-\mathrm{i}\Delta k_z L}, \tag{9}$$

where

$$\begin{aligned}
G_1 &= \mathrm{e}^{\delta aL}[\cosh(\xi L) + \frac{a}{\xi}\sinh(\xi L)],\\
G_2 &= \mathrm{e}^{\delta aL}[\cosh(\xi L) - \frac{a}{\xi}\sinh(\xi L)],\\
g_1 &= \frac{a_{\text{pc}}}{\xi}\mathrm{e}^{\delta aL}\sinh(\xi L), \quad g_2 = -\frac{a_{\text{cp}}}{\xi}\mathrm{e}^{\delta aL}\sinh(\xi L), \qquad (10)
\end{aligned}$$

with

$$\begin{aligned}
&a_{\text{p}j} = \mathrm{i}k_{\text{p}}\chi_{\text{p}j}/2,\ \ a_{\text{c}j} = \mathrm{i}k_{\text{c}}\chi_{\text{c}j}^{*}/2 \quad (j = \text{p},\text{c}),\\
&a = (a_{\text{pp}} + a_{\text{cc}} - \mathrm{i}\Delta k_z)/2, \quad \xi = \sqrt{a^2 - a_{\text{pc}}a_{\text{cp}}},\\
&\delta a = (a_{\text{pp}} - a_{\text{cc}} + \mathrm{i}\Delta k_z)/2. \qquad (11)
\end{aligned}$$

The number operators of the probe beam and conjugate beam are defined as $\hat{N}_{\text{p}} = \hat{\mathcal{E}}_{\text{p}}^{\dagger}\hat{\mathcal{E}}_{\text{p}}$ and $\hat{N}_{\text{c}} = \hat{\mathcal{E}}_{\text{c}}^{\dagger}\hat{\mathcal{E}}_{\text{c}}$, respectively. From the above result, we define the gain of the probe beam in the 4WM process as

$$G_{\text{p}} = \frac{\langle\hat{N}_{\text{p}}\rangle_{\text{out}}}{\langle\hat{N}_{\text{p}}\rangle_{\text{in}}} \simeq |G_1|^2, \tag{12}$$

where the initial condition is $\langle\hat{N}_{\text{p}}\rangle_{\text{in}} \gg 1$ and $\langle\hat{N}_{\text{c}}\rangle_{\text{in}} = 0$. The 4WM generates a correlated probe and conjugate beams, and the relative intensity fluctuations are reduced for the amplification process. After the 4WM, the relative intensity fluctuation is given by

$$\begin{aligned}
\Delta^2(\hat{N}_{\text{p}} - \hat{N}_{\text{c}})_{\text{out}} &= (|G_1|^2 - |g_2|^2)^2\Delta^2(\hat{N}_{\text{p}})_{\text{in}}\\
&\quad + |g_1^{*}G_1 - g_2^{*}G_2|^2[\langle\hat{N}_{\text{p}}\rangle_{\text{in}} + 1]. \qquad (13)
\end{aligned}$$

Hence the beams have been amplified without increasing the relative intensity noise, and they are relative intensity squeezed. The standard quantum limit (SQL) is a differential measurement equal to the total optical power, that is,

$$\langle\hat{N}_{\text{p}} - \hat{N}_{\text{c}}\rangle_{\text{SQL}} \equiv \langle\hat{N}_{\text{p}} + \hat{N}_{\text{c}}\rangle \simeq (|G_1|^2 + |g_2|^2)\langle\hat{N}_{\text{p}}\rangle_{\text{in}}. \tag{14}$$

The noise figure of the process (or "degree of squeezing") is the ratio of the measured noise to the corresponding shot-noise level for equal optical power. The typical noise figure is quoted as the noise in decibels relative to the SQL.

3. Phase matching angles

In this section, we describe how to obtain the optimal angles θ_1 and θ_2 between the probe field and two non-collinear pump fields when the angle θ_0 between pump fields P_1 and P_2 is given.

As shown in Fig. 4(a), when two pump fields E_{P_1} and E_{P_2} are incident at an angle, the total projection of the wavevector of the pump fields onto the z-axis is $2\boldsymbol{k}_{\text{P}_Z}$ and becomes smaller;

i.e., $2|\boldsymbol{k}_{\mathrm{P}_Z}| < |\boldsymbol{k}_{\mathrm{P}_1}| + |\boldsymbol{k}_{\mathrm{P}_2}|$. The geometric phase matching condition (GPMC) is given by

$$\begin{aligned}\Delta k_z &= |\boldsymbol{k}_{\mathrm{P}_1}|\cos(\theta_{z1}) + |\boldsymbol{k}_{\mathrm{P}_2}|\cos(\theta_{z2}) - (|\boldsymbol{k}_{\mathrm{p}}| + |\boldsymbol{k}_{\mathrm{c}}|)\cos\theta_3 \\ &= 2|\boldsymbol{k}_{\mathrm{P}_Z}| - (|\boldsymbol{k}_{\mathrm{p}}| + |\boldsymbol{k}_{\mathrm{c}}|)\cos\theta_3, \end{aligned} \tag{15}$$

where θ_3 is the angle between the probe and the projected pump field. In fact, if the 4WM is efficient, the GPMC of Eq. (15) may not be satisfied, but the effective phase matching condition (EPMC) must be met:

$$\boldsymbol{k}_{\mathrm{P}_1} + \boldsymbol{k}_{\mathrm{P}_2} - n_{\mathrm{p}}\boldsymbol{k}_{\mathrm{p}} - n_{\mathrm{c}}\boldsymbol{k}_{\mathrm{c}} = 0, \tag{16}$$

where the refractive index $n_{\mathrm{p}} = \sqrt{1+\mathrm{Re}(\chi_{\mathrm{pp}})}$, and $n_{\mathrm{c}} = \sqrt{1+\mathrm{Re}(\chi_{\mathrm{cc}})}$. For the case of two non-collinear pump fields, equation (16) can be written as

$$\cos\theta_3 = \frac{\omega_{\mathrm{P}_1}\cos(\theta_{z1}) + \omega_{\mathrm{P}_2}\cos(\theta_{z2})}{n_{\mathrm{p}}\omega_{\mathrm{p}} + n_{\mathrm{c}}\omega_{\mathrm{c}}}. \tag{17}$$

Using the conservation of energy condition $\omega_{\mathrm{p}} + \omega_{\mathrm{c}} = \omega_{\mathrm{P}_1} + \omega_{\mathrm{P}_2} = 2\omega_0$, where ω_0 is the frequency of the pump field, and considering $\theta_{z1} = \theta_{z2} = \theta_0/2$, equation (17) is written as

$$\cos\theta_3 = \frac{2\omega_0\cos(\theta_0/2)}{n_{\mathrm{p}}\omega_{\mathrm{p}} + \omega_{\mathrm{c}}}, \tag{18}$$

where $n_{\mathrm{c}} \simeq 1$ due to the conjugate field with a large detuning. For a given angle θ_0, when $n_{\mathrm{p}} = 1$, the EPMC of Eq. (18) imposes $\theta_3 = \theta_0/2$. Under this condition, the GPMC $\Delta k_z = 0$ is also satisfied, which is the phase matching condition in free space, where the beams are required rigorously co-propagating as shown in Fig. 4(b).

When $n_{\mathrm{p}} > 1$, the EPMC of Eq. (18) is established to require $\theta_3 > \theta_0/2$, which means that the GPMC of Eq. (15) cannot be satisfied and will occur $\Delta k_z > 0$, as shown in Fig. 4(c). Considering $\theta_1 = \theta_2 = \theta$ and using the law of cosines we obtain the angle requirement between the probe field and the pump fields

$$\theta > \cos^{-1}\left[\frac{1+\cos\theta_0}{2}\right]. \tag{19}$$

If $n_{\mathrm{p}} < 1$, similarly, the EPMC of Eq. (18) requires $\theta_3 < \theta_0/2$ and imposes $\Delta k_z < 0$, as shown in Fig. 4(d). In addition, the generated probe and conjugate beams have separate directions, which requires that the angle $\theta_3 > 0$. Furthermore, using the minimum value of the refractive index $\min(n_{\mathrm{p}})$ according to Eq. (18), we obtain

$$0 < (\theta_3)_{\min} < \theta_3 < \frac{\theta_0}{2}, \tag{20}$$

where $(\theta_3)_{\min} = \cos^{-1}\left[2\omega_0\cos(\theta_0/2)/(\min(n_{\mathrm{p}})\omega_{\mathrm{p}} + \omega_{\mathrm{c}})\right]$ and correspondingly,

$$\frac{\theta_0}{2} < \theta_{\min} < \theta < \cos^{-1}\left[\frac{1+\cos\theta_0}{2}\right], \tag{21}$$

where $\theta_{\min} = \cos^{-1}\left[\omega_0(1+\cos\theta_0)/(\min(n_{\mathrm{p}})\omega_{\mathrm{p}} + \omega_{\mathrm{c}})\right]$. For the case of collinear pump fields, the angle θ_0 here is equivalent to 0, where the condition $\theta_3 < \theta_0/2$ cannot be satisfied because θ_3 cannot be less than 0. That is, when $n_{\mathrm{p}} < 1$, the EPMC cannot be satisfied for 4WM driven by a single pump field. Compared to the collinear pump fields case, this is a new region.

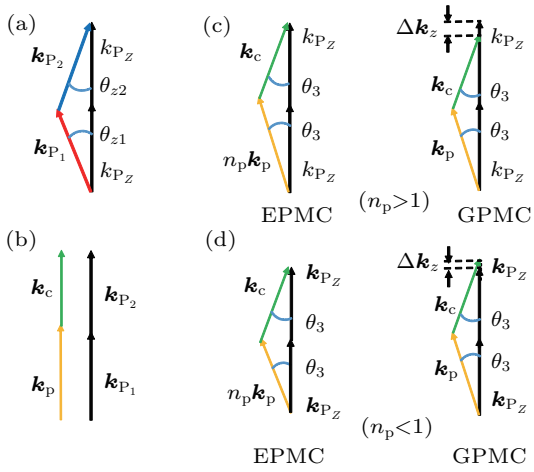


Fig. 4. (a) The wavevectors $\boldsymbol{k}_{\mathrm{P}_1}$ and $\boldsymbol{k}_{\mathrm{P}_2}$ are projected onto the axis as $2\boldsymbol{k}_{\mathrm{P}_Z}$. The angles between the $\boldsymbol{k}_{\mathrm{P}_Z}$ and the pump fields $\boldsymbol{k}_{\mathrm{P}_1}$ and $\boldsymbol{k}_{\mathrm{P}_2}$ are θ_{z1} and θ_{z2}, respectively. (b) The configuration in which the geometric phase matching condition (GPMC) is fulfilled. The configuration in which the effective phase matching condition (EPMC) is fulfilled for an effective index of refraction of the probe (c) $n_{\mathrm{p}} > 1$ and (d) $n_{\mathrm{p}} < 1$, with necessary geometric mismatches of (c) $\Delta k_z > 0$ and (d) $\Delta k_z < 0$, respectively.

For degenerate case, the form of Eqs. (15)–(17) is the same except for the magnitude of the wave vectors. With two strong beams with the frequency of the probe and conjugate beams, and along the direction of them, and a week beam having the frequency and direction of the previous pump, we can generate the frequency degenerate and spatial nondegenerate twin beams by changing the detunings of Δ_1 and Δ_2. Similar to the non-degenerate case, if $n_{\mathrm{p}} + n_{\mathrm{c}} = 2$, then GPMC $\Delta k_z = 0$ will be satisfied. If $n_{\mathrm{p}} + n_{\mathrm{c}} > 2$ or $n_{\mathrm{p}} + n_{\mathrm{c}} < 2$, then the corresponding GPMC $\Delta k_z > 0$ or $\Delta k_z < 0$ will also be obtained.

4. Gain comparison

In this section, we numerically analyze the gain of the frequency non-degenerate squeezed light, and describe the phase matching between the $n_{\mathrm{p}} > 1$ and $n_{\mathrm{p}} < 1$ by an angle adjustment.

In our non-degenerate experiment,[56] the state $|g,m\rangle$ (or state $|1,2\rangle$) involves the hyperfine levels $|5\mathrm{S}_{1/2}, F = 2,3\rangle$, where the hyperfine splitting of the ground state is $\omega_{21} = 2\pi \times 3.035$ GHz, and the excited state $|e\rangle$ (or state $|3,4\rangle$) is $|5P_{1/2}\rangle$ has an excited state decay rate of $\gamma = 2\pi \times 5.75$ MHz. The pump field is blue-detuned approximately 1 GHz to the D1 line of Rb-85 $5\mathrm{S}_{1/2} \rightarrow 5\mathrm{P}_{1/2}$. The powers of the pump fields E_{P_1} and E_{P_2} are set to 350 mW, and their waists at the crossing point are 622 μm and 596 μm, respectively. The Rabi

frequencies of Ω_{P_1} and Ω_{P_2} are $\Omega_{P_1} \simeq 28\gamma$ and $\Omega_{P_2} \simeq 30\gamma$ for an effective electric dipole $d = 1.47 \times 10^{-29}$ Cm.[62] The atomic number density of Rb-85 at 125 °C is approximately $N \simeq 4.5 \times 10^{18}$ m^{-3}.

Figures 5(a) and 5(b) show the direct susceptibilities χ_{pp} and χ_{cc} for the probe and conjugate fields as a function of the two-photon detuning δ/γ, and we obtain that χ_{cc} is far less than χ_{pp} due to large detuning. In Fig. 5(a), when $\delta < 0$, the real part of χ_{pp} is effectively responsible for the index of refraction of the probe for the single pump field case.[57,59] However, for our two-pump-fields input case, the phase matching condition can also be satisfied on the other side $\delta > 0$.

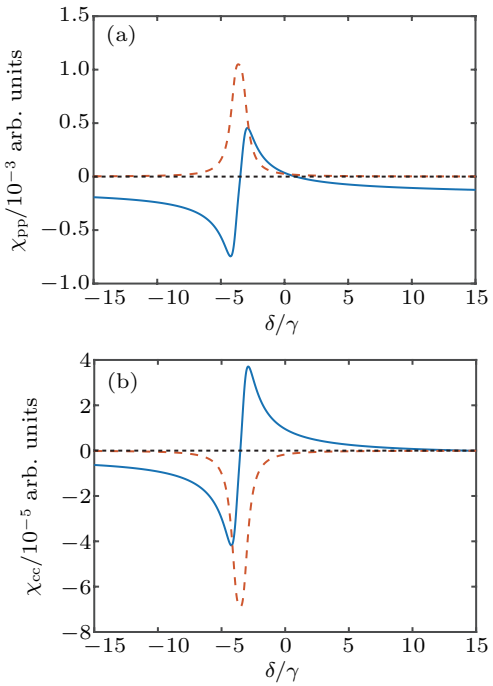


Fig. 5. The direct and cross susceptibilities for the probe and conjugate fields as a function of the two-photon detuning δ/γ. The solid lines are the real parts, and the dashed lines are the imaginary parts. The excited state decay rate is $\gamma = 2\pi \times 5.75$ MHz, and $\gamma_c = 0.5\gamma$. The hyperfine splitting of the ground state is $\omega_{21} = 2\pi \times 3.035$ GHz. The detuning of pump 1 is $\Delta_1 = 174\gamma$. The Rabi frequencies of Ω_{P_1} and Ω_{P_2} are $\Omega_{P_1} = 28\gamma$ and $\Omega_{P_2} = 30\gamma$, respectively.

According to Eq. (12), we plot the probe gain G_p as a function of the two-photon detuning δ and the geometric phase mismatch Δk_z in the presence of a single pump field and two pump fields, as shown in Fig. 6. One can see that the maximum gains are obtained on the side $\delta < 0$ with $\Delta k_z > 0$, for both the cases. When $\Delta k_z < 0$, the probe gain G_p does not exist for the single pump field input case and only occurs for the two-pump-fields input case. The bandwidth of the probe gain is relatively large due to the slow change in the refractive index with the two-photon detuning.

The theoretical output probe gain G_p as a function of the two-photon detuning δ/γ and the probe-pump angle θ with (a) a single pump field and (b) two pump fields is shown in Fig. 7, where we consider $\boldsymbol{k}_{P_1} = \boldsymbol{k}_{P_2} = \boldsymbol{k}_P$ and $\theta_1 = \theta_2 = \theta$. It can be seen that for a single pump field, the gain and 4WM process are on the $\delta < 0$ side as the angle θ increases due to phase matching. For the case of two pump fields, the gain and 4WM process can be achieved on the left side (line L_2) or the right side (line L_0 or line L_1) by choosing the angle θ between the probe field and the pump fields when the angle θ_0 is given.

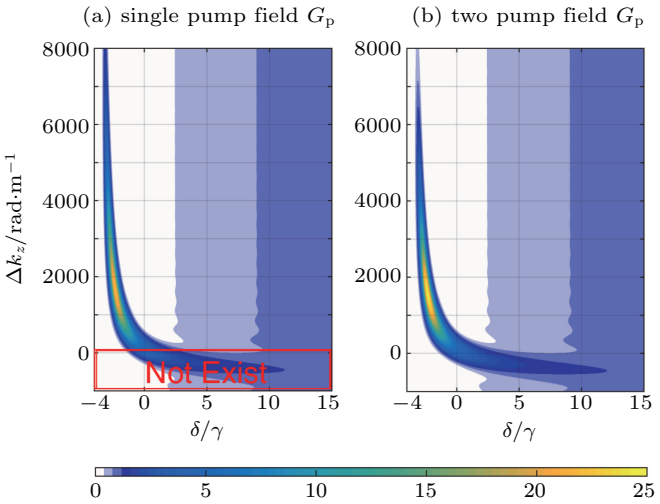


Fig. 6. Theoretical output probe gain G_p as a function of the two-photon detuning δ/γ and the geometrical phase match Δk_z with (a) a single pump field and (b) two pump fields. Here the excited state decay rate is $\gamma = 2\pi \times 5.75$ MHz, the decoherence rate is $\gamma_c = 0.5\gamma$, the atom density is $N = 4.5 \times 10^{18}$ m^{-3}, the length of the medium is $L = 12.5$ mm and the pump Rabi frequencies are $\Omega_{P_1} = 28\gamma$ and $\Omega_{P_2} = 30\gamma$.

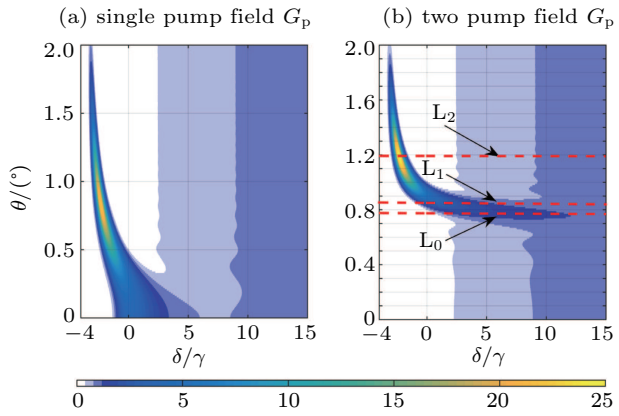


Fig. 7. Theoretical output probe gain G_p as a function of the two-photon detuning δ/γ and the probe-pump angle θ with (a) a single pump field and (b) two pump fields. The area intersecting the dashed line is the area selected by our experimental parameters. The angle between pump fields P_1 and P_2 is $\theta_0/2 = 0.615°$. The angles between the probe field and the pump fields P_1 and P_2 are $\theta_1 = \theta_2 = \theta = 0.861°$.

The area intersecting the dashed line L_1 in Fig. 7(b) is the area selected by our experimental parameters, where $\theta_0/2 = 0.615°$, and $\theta = 0.861°$. According to the minimum value $\min(\mathrm{Re}(\chi_{pp})) = -1.609 \times 10^{-4}$ in Fig. 6, using Eq. (21), we obtain

$$0.7630° < \theta < 0.8697°. \tag{22}$$

If we only choose the angle θ based on the bandwidth, we can choose line L_0 [Fig. 7(b)] because it has the largest band-

width. However, in the experiment, the angle is finely adjusted according to the degree of squeezing, and the optimum value of the angle θ is different. If the angle θ is chosen as 1.2° of line L_2 in Fig. 7(b), the 4WM process driven by two pump fields will also be observed on the $\delta < 0$ side due to the large gain. On the other hand, when the probe-pump angle θ is 1.2°, the 4WM processes independently generated by the pump field E_{P_1} and pump field E_{P_2} can occur and two conjugate fields c_1 and c_2 can also be observed, because of their gains as shown in Fig. 7(a). Therefore, the strong conjugate field c and two weak conjugate fields c_1 and c_2 may all occur under the condition of $\theta \sim 1.2°$ and $\delta < 0$. That is a two-pump forward phase-matching geometry and every single-pump phase-matching condition is satisfied.[60] However, in this region, the absorption is also large, which will affect the degree of squeezing of the two generated beams.

Here θ_0 has a fundamental effect on wavevector matching in the new 4WM process, thus opening up a region in which high-intensity-difference squeezed light can be obtained over a wide bandwidth with low loss and moderate gain. The gain curve in Fig. 7(b) shifts upward as the angle θ_0 increases, because the minimum value of the angle θ is greater than the angle $\theta_0/2$.

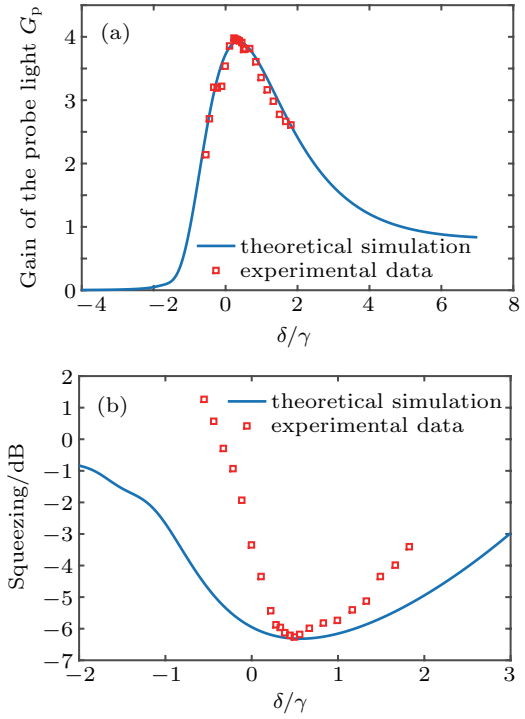


Fig. 8. The gain of the probe field (a) and the squeezing (b) as a function of the two-photon detuning δ. The parameters are as follows: $\gamma = 2\pi \times 5.75$ MHz, $\gamma_c = 0.5\gamma$, $N = 4.5 \times 10^{18}$ m^{-3}, $L = 12.5$ mm, $\Omega_{P_1} = 28\gamma$, $\Omega_{P_2} = 30\gamma$, $\theta_0/2 = 0.615°$, and $\theta_1 = \theta_2 = 0.861°$.

The gain of the probe field and the squeezing as a function of the two-photon detuning δ is shown in Fig. 8, where the square represents the experimental data from Ref. [56] and the solid line is a theoretical simulation. The theoretical simulations and experimental data of the gain of the probe field are in good agreement, as shown in Fig. 8(a). In the experiment, the intensity-difference-squeezed light for the nondegenerate case with quantum noise almost 7 dB reduction was generated.[56] The squeezing degree is affected by the spatial mode mismatch, optical absorption by the atomic system, optical loss in the light path, and atomic decoherence. Figure 8(b) shows the theoretical simulations and experimental data of squeezing, where the theoretical squeezing curve is reduced by 0.56 times and the agreement is not very good because these effects are not included in our model in order to clarify the physics picture concisely. The bandwidth of the gain is relatively larger than that for the single pump field case, which is advantageous for realizing wide-bandwidth frequency-degenerate and nondegenerate intensity-squeezed light. These light fields can be widely used in quantum information and other fields.

5. Conclusion

We have studied that a two-mode squeezed light is generated from a 4WM process driven by two pump fields crossing a small angle, where the twin beams are generated with a new phase matching condition. Different from 4WM realized by a single pump field where the gain peak can only be achieved on the $\delta < 0$ side, the new 4WM process is implemented from the $\delta < 0$ side to the $\delta > 0$ side by an angle adjustment. The refractive index of the corresponding probe field n_p can be converted from $n_p > 1$ to $n_p < 1$, which can also be used to convert between slow light[63] and fast light.[64] On the $n_p < 1$ side, the refractive index n_p changes slowly with the two-photon detuning δ over a large range, which leads to a relatively large gain bandwidth. With an exchange of the roles of the pump and probe beams, the frequency degenerate and spatial nondegenerate twin beams can be generated. This type of twin beams can be combined and interfered directly on the beam splitter, and can be applied in quantum information and quantum metrology.

Appendix A: Susceptibilities with two pump fields crossing a small angle input

As shown in Fig. 3, we assume that the two pump fields E_{P_1} and E_{P_2} couple the transitions $|1\rangle \to |3\rangle$ and $|2\rangle \to |4\rangle$, respectively. The probe field couples the transition $|2\rangle \to |3\rangle$, and the conjugate field couples the transition $|1\rangle \to |4\rangle$. The transitions $|1\rangle \to |2\rangle$ and $|3\rangle \to |4\rangle$ are not dipole allowed transitions.

Consequently, we obtain the following set of equations for the populations σ_{nn}:

$$\frac{\partial \sigma_{11}}{\partial t} = \Gamma_{13}\sigma_{33} + \Gamma_{14}\sigma_{44} + \mathrm{i}(\Omega_{P_1}^{*}\, \mathrm{e}^{-\mathrm{i}\boldsymbol{k}_{P_1}\cdot\boldsymbol{r}}\tilde{\sigma}_{13} + g_c\hat{\mathcal{E}}_c^{\dagger} \times \mathrm{e}^{-\mathrm{i}\boldsymbol{k}_c\cdot\boldsymbol{r}}\tilde{\sigma}_{14} - \Omega_{P_1}\, \mathrm{e}^{\mathrm{i}\boldsymbol{k}_{P_1}\cdot\boldsymbol{r}}\tilde{\sigma}_{31} - g_c\hat{\mathcal{E}}_c\, \mathrm{e}^{\mathrm{i}\boldsymbol{k}_c\cdot\boldsymbol{r}}\tilde{\sigma}_{41}), \tag{A1}$$

$$\frac{\partial\sigma_{22}}{\partial t}=\Gamma_{23}\sigma_{33}+\Gamma_{24}\sigma_{44}+\mathrm{i}(\Omega_{\mathrm{P}_2}^{*}\,\mathrm{e}^{-\mathrm{i}\boldsymbol{k}_{\mathrm{P}_2}\cdot\boldsymbol{r}}\tilde{\sigma}_{24}+g_{\mathrm{p}}\hat{\mathcal{E}}_{\mathrm{p}}^{\dagger}\times\mathrm{e}^{-\mathrm{i}\boldsymbol{k}_{\mathrm{p}}\cdot\boldsymbol{r}}\tilde{\sigma}_{23}-\Omega_{\mathrm{P}_2}\,\mathrm{e}^{\mathrm{i}\boldsymbol{k}_{\mathrm{P}_2}\cdot\boldsymbol{r}}\tilde{\sigma}_{42}-g_{\mathrm{p}}\hat{\mathcal{E}}_{\mathrm{p}}\,\mathrm{e}^{\mathrm{i}\boldsymbol{k}_{\mathrm{p}}\cdot\boldsymbol{r}}\tilde{\sigma}_{32}),\tag{A2}$$

$$\frac{\partial\sigma_{33}}{\partial t}=-\Gamma_{3}\sigma_{33}+\mathrm{i}(\Omega_{\mathrm{P}_1}\,\mathrm{e}^{\mathrm{i}\boldsymbol{k}_{\mathrm{P}_1}\cdot\boldsymbol{r}}\tilde{\sigma}_{31}+g_{\mathrm{p}}\hat{\mathcal{E}}_{\mathrm{p}}\,\mathrm{e}^{\mathrm{i}\boldsymbol{k}_{\mathrm{p}}\cdot\boldsymbol{r}}\tilde{\sigma}_{32}-\Omega_{\mathrm{P}_1}^{*}\,\mathrm{e}^{-\mathrm{i}\boldsymbol{k}_{\mathrm{P}_1}\cdot\boldsymbol{r}}\tilde{\sigma}_{13}-g_{\mathrm{p}}\hat{\mathcal{E}}_{\mathrm{p}}^{\dagger}\,\mathrm{e}^{-\mathrm{i}\boldsymbol{k}_{\mathrm{p}}\cdot\boldsymbol{r}}\tilde{\sigma}_{23}),\tag{A3}$$

$$\frac{\partial\sigma_{44}}{\partial t}=-\Gamma_{4}\sigma_{44}+\mathrm{i}(\Omega_{\mathrm{P}_2}\,\mathrm{e}^{\mathrm{i}\boldsymbol{k}_{\mathrm{P}_2}\cdot\boldsymbol{r}}\tilde{\sigma}_{42}+g_{\mathrm{c}}\hat{\mathcal{E}}_{\mathrm{c}}\,\mathrm{e}^{\mathrm{i}\boldsymbol{k}_{\mathrm{c}}\cdot\boldsymbol{r}}\tilde{\sigma}_{41}-\Omega_{\mathrm{P}_2}^{*}\,\mathrm{e}^{-\mathrm{i}\boldsymbol{k}_{\mathrm{P}_2}\cdot\boldsymbol{r}}\tilde{\sigma}_{24}-g_{\mathrm{c}}\hat{\mathcal{E}}_{\mathrm{c}}^{\dagger}\,\mathrm{e}^{-\mathrm{i}\boldsymbol{k}_{\mathrm{c}}\cdot\boldsymbol{r}}\tilde{\sigma}_{14}),\tag{A4}$$

where Γ_{mn} is the population decay rate from the level n to level m, and we introduce slowly varying matrix elements in time: $\sigma_{13}=\tilde{\sigma}_{13}\,\mathrm{e}^{-\mathrm{i}\omega_{\mathrm{p}1}t}$, $\sigma_{14}=\tilde{\sigma}_{14}\,\mathrm{e}^{-\mathrm{i}\omega_{\mathrm{c}}t}$, $\sigma_{24}=\tilde{\sigma}_{24}\,\mathrm{e}^{-\mathrm{i}\omega_{\mathrm{p}2}t}$, and $\sigma_{23}=\tilde{\sigma}_{23}\,\mathrm{e}^{-\mathrm{i}\omega_{\mathrm{p}}t}$. In addition, the set of equations for $\tilde{\sigma}_{nm}$ ($n\neq m$) are given by

$$\frac{\partial\tilde{\sigma}_{42}}{\partial t}=[\mathrm{i}(\delta-\Delta_2)-\gamma_{42}]\tilde{\sigma}_{42}-\mathrm{i}[\Omega_{\mathrm{P}_2}^{*}\,\mathrm{e}^{-\mathrm{i}\boldsymbol{k}_{\mathrm{P}_2}\cdot\boldsymbol{r}}\sigma_{22,44}-g_{\mathrm{p}}\hat{\mathcal{E}}_{\mathrm{p}}^{\dagger}\,\mathrm{e}^{-\mathrm{i}\boldsymbol{k}_{\mathrm{p}}\cdot\boldsymbol{r}}\tilde{\sigma}_{43}+g_{\mathrm{c}}\hat{\mathcal{E}}_{\mathrm{c}}^{\dagger}\,\mathrm{e}^{-\mathrm{i}\boldsymbol{k}_{\mathrm{c}}\cdot\boldsymbol{r}}\tilde{\sigma}_{12}],\tag{A5}$$

$$\frac{\partial\tilde{\sigma}_{41}}{\partial t}=(-\mathrm{i}\Delta_2-\gamma_{41})\tilde{\sigma}_{41}+\mathrm{i}[\Omega_{\mathrm{P}_1}^{*}\,\mathrm{e}^{-\mathrm{i}\boldsymbol{k}_{\mathrm{P}_1}\cdot\boldsymbol{r}}\tilde{\sigma}_{43}-g_{\mathrm{c}}\hat{\mathcal{E}}_{\mathrm{c}}^{\dagger}\,\mathrm{e}^{-\mathrm{i}\boldsymbol{k}_{\mathrm{c}}\cdot\boldsymbol{r}}\sigma_{11,44}-\Omega_{\mathrm{P}_2}^{*}\,\mathrm{e}^{-\mathrm{i}\boldsymbol{k}_{\mathrm{P}_2}\cdot\boldsymbol{r}}\tilde{\sigma}_{12}],\tag{A6}$$

$$\frac{\partial\tilde{\sigma}_{32}}{\partial t}=[\mathrm{i}(\delta-\Delta_1)-\gamma_{32}]\tilde{\sigma}_{32}+\mathrm{i}[\Omega_{\mathrm{P}_2}^{*}\,\mathrm{e}^{-\mathrm{i}\boldsymbol{k}_{\mathrm{P}_2}\cdot\boldsymbol{r}}\tilde{\sigma}_{34}-g_{\mathrm{p}}\hat{\mathcal{E}}_{\mathrm{p}}^{\dagger}\,\mathrm{e}^{-\mathrm{i}\boldsymbol{k}_{\mathrm{p}}\cdot\boldsymbol{r}}\sigma_{22,33}-\Omega_{\mathrm{P}_1}^{*}\,\mathrm{e}^{-\mathrm{i}\boldsymbol{k}_{\mathrm{P}_1}\cdot\boldsymbol{r}}\tilde{\sigma}_{12}],\tag{A7}$$

$$\frac{\partial\tilde{\sigma}_{31}}{\partial t}=-(\mathrm{i}\Delta_1+\gamma_{31})\tilde{\sigma}_{31}-\mathrm{i}[\Omega_{\mathrm{P}_1}^{*}\,\mathrm{e}^{-\mathrm{i}\boldsymbol{k}_{\mathrm{P}_1}\cdot\boldsymbol{r}}\sigma_{11,33}-g_{\mathrm{c}}\hat{\mathcal{E}}_{\mathrm{c}}^{\dagger}\times\mathrm{e}^{-\mathrm{i}\boldsymbol{k}_{\mathrm{c}}\cdot\boldsymbol{r}}\tilde{\sigma}_{34}+g_{\mathrm{p}}\hat{\mathcal{E}}_{\mathrm{p}}^{\dagger}\,\mathrm{e}^{-\mathrm{i}\boldsymbol{k}_{\mathrm{p}}\cdot\boldsymbol{r}}\tilde{\sigma}_{21}],\tag{A8}$$

$$\frac{\partial\tilde{\sigma}_{43}}{\partial t}=[\mathrm{i}(\Delta_1-\Delta_2)-\gamma_{43}]\tilde{\sigma}_{43}+\mathrm{i}[\Omega_{\mathrm{P}_1}\,\mathrm{e}^{\mathrm{i}\boldsymbol{k}_{\mathrm{P}_1}\cdot\boldsymbol{r}}\tilde{\sigma}_{41}+g_{\mathrm{p}}\hat{\mathcal{E}}_{\mathrm{p}}\times\mathrm{e}^{\mathrm{i}\boldsymbol{k}_{\mathrm{p}}\cdot\boldsymbol{r}}\tilde{\sigma}_{42}-\Omega_{\mathrm{P}_2}^{*}\,\mathrm{e}^{-\mathrm{i}\boldsymbol{k}_{\mathrm{P}_2}\cdot\boldsymbol{r}}\tilde{\sigma}_{23}-g_{\mathrm{c}}\hat{\mathcal{E}}_{\mathrm{c}}^{\dagger}\,\mathrm{e}^{-\mathrm{i}\boldsymbol{k}_{\mathrm{c}}\cdot\boldsymbol{r}}\tilde{\sigma}_{13}],\tag{A9}$$

$$\frac{\partial\tilde{\sigma}_{21}}{\partial t}=-(\mathrm{i}\delta+\gamma_{21})\tilde{\sigma}_{21}+\mathrm{i}[\Omega_{\mathrm{P}_1}^{*}\,\mathrm{e}^{-\mathrm{i}\boldsymbol{k}_{\mathrm{P}_1}\cdot\boldsymbol{r}}\tilde{\sigma}_{23}+g_{\mathrm{c}}\hat{\mathcal{E}}_{\mathrm{c}}^{\dagger}\tilde{\sigma}_{24}\times\mathrm{e}^{-\mathrm{i}\boldsymbol{k}_{\mathrm{c}}\cdot\boldsymbol{r}}-\Omega_{\mathrm{P}_2}\,\mathrm{e}^{\mathrm{i}\boldsymbol{k}_{\mathrm{P}_2}\cdot\boldsymbol{r}}\tilde{\sigma}_{41}-g_{\mathrm{p}}\hat{\mathcal{E}}_{\mathrm{p}}\,\mathrm{e}^{\mathrm{i}\boldsymbol{k}_{\mathrm{p}}\cdot\boldsymbol{r}}\tilde{\sigma}_{31}],\tag{A10}$$

where $\sigma_{22,44}=\sigma_{22}-\sigma_{44}$, $\sigma_{11,44}=\sigma_{11}-\sigma_{44}$, $\sigma_{22,33}=\sigma_{22}-\sigma_{33}$, and $\sigma_{11,33}=\sigma_{11}-\sigma_{33}$, the single-photon detunings are $\Delta_1=\omega_{\mathrm{P}_1}-\omega_{31}$ and $\Delta_2=\omega_{\mathrm{P}_2}-\omega_{42}+\delta$, the two-photon detuning is $\delta=\omega_{\mathrm{P}_1}-\omega_{\mathrm{p}}-\omega_{21}$, and the slowly varying matrix elements are $\sigma_{43}=\tilde{\sigma}_{43}\,\mathrm{e}^{\mathrm{i}(\omega_{\mathrm{p}2}-\omega_{\mathrm{p}})t}$ and $\sigma_{12}=\tilde{\sigma}_{12}\,\mathrm{e}^{-\mathrm{i}(\omega_{\mathrm{c}}-\omega_{\mathrm{p}2})t}$; γ_{nm} gives the dephasing rate of the σ_{nm} coherence, and $\gamma_{nm}=(\Gamma_m+\Gamma_n)/2+\gamma_{nm}^{c}$, where Γ_n is the total decay rate out of level n and γ_{nm}^{c} is the dephasing rate due to any other source of decoherence.

Now we are in a position to solve the properties of the system. For convenience, we let $\Gamma_3=\Gamma_4\equiv\gamma$ and $\Gamma_{13}=\Gamma_{14}=\Gamma_{23}=\Gamma_{24}=\gamma/2$, and the complex decay rates are

$$\xi_{42}=-\gamma/2+\mathrm{i}(\delta-\Delta_2),\ \ \xi_{41}=-(\gamma/2+\mathrm{i}\Delta_2),\tag{A11}$$

$$\xi_{32}=-\gamma/2+\mathrm{i}(\delta-\Delta_1),\ \ \xi_{31}=-(\gamma/2+\mathrm{i}\Delta_1),\tag{A12}$$

$$\xi_{43}=-\gamma+\mathrm{i}(\Delta_1-\Delta_2),\ \ \xi_{21}=-(\gamma_{21}+\mathrm{i}\delta).\tag{A13}$$

In order to obtain analytical expressions, we assume that the pump fields propagate without depletion, and the steady-state expectation values for the zeroth-order atomic operators σ_{33} and σ_{44} are equal to

$$\langle\sigma_{33}\rangle=\langle\sigma_{44}\rangle=\frac{|\Omega_{\mathrm{P}_1}|^2|\Omega_{\mathrm{P}_2}|^2}{|\Omega_{\mathrm{P}_2}|^2|\xi_{31}|^2+|\Omega_{\mathrm{P}_1}|^2|\xi_{42}|^2+4|\Omega_{\mathrm{P}_1}|^2|\Omega_{\mathrm{P}_2}|^2}.\tag{A14}$$

Then, the population differences are given by

$$\langle\sigma_{11,33}\rangle=\langle\sigma_{11,44}\rangle=\frac{|\xi_{31}|^2|\Omega_{\mathrm{P}_2}|^2}{|\Omega_{\mathrm{P}_2}|^2|\xi_{31}|^2+|\Omega_{\mathrm{P}_1}|^2|\xi_{42}|^2+4|\Omega_{\mathrm{P}_1}|^2|\Omega_{\mathrm{P}_2}|^2},\tag{A15}$$

$$\langle\sigma_{22,33}\rangle=\langle\sigma_{22,44}\rangle=\frac{|\xi_{42}|^2|\Omega_{\mathrm{P}_1}|^2}{|\xi_{31}|^2|\Omega_{\mathrm{P}_2}|^2+|\xi_{42}|^2|\Omega_{\mathrm{P}_1}|^2+4|\Omega_{\mathrm{P}_1}\Omega_{\mathrm{P}_2}|^2}.\tag{A16}$$

We also assume that the probe and conjugate fields are weak fields, such that we only keep terms to first order in Ω_{p} and Ω_{c}. The steady-state density matrix elements $\tilde{\sigma}_{23}$ and $\tilde{\sigma}_{14}$ are given by

$$\begin{aligned}\tilde{\sigma}_{23}=\frac{\mathrm{i}\xi_{41}}{D}\times\{&g_{\mathrm{p}}\hat{\mathcal{E}}_{\mathrm{p}}\,\mathrm{e}^{\mathrm{i}\boldsymbol{k}_{\mathrm{p}}\cdot\boldsymbol{r}}[\sigma_{11,33}\left(\frac{\xi_{43}}{\xi_{31}}+\frac{|\Omega_{\mathrm{P}_1\mathrm{P}2}|^2}{\xi_{31}\xi_{41}}\right)|\Omega_{\mathrm{P}_1}|^2\\&-(\frac{\xi_{43}|\Omega_{\mathrm{P}_2}|^2+\xi_{21}|\Omega_{\mathrm{P}_1}|^2}{\xi_{41}}+\xi_{21}\xi_{43})\sigma_{22,33}+|\Omega_{\mathrm{P}_2}|^2\\&\times\left(\frac{\xi_{21}}{\xi_{42}}-\frac{|\Omega_{\mathrm{P}_1\mathrm{P}2}|^2}{\xi_{42}\xi_{41}}\right)\sigma_{22,44}]+\Omega_{\mathrm{P}_1}\Omega_{\mathrm{P}_2}[\frac{\xi_{21}+\xi_{43}}{\xi_{41}}\sigma_{11,44}\\&+\left(\frac{\xi_{43}}{\xi_{42}^{*}}+\frac{|\Omega_{\mathrm{P}_1\mathrm{P}2}|^2}{\xi_{42}^{*}\xi_{41}}\right)\sigma_{22,44}\\&+\left(\frac{\xi_{21}}{\xi_{31}^{*}}-\frac{|\Omega_{\mathrm{P}_1\mathrm{P}2}|^2}{\xi_{31}^{*}\xi_{41}}\right)\sigma_{11,33}]\,\mathrm{e}^{\mathrm{i}\Delta\boldsymbol{k}_{\mathrm{p}}\cdot\boldsymbol{r}}g_{\mathrm{c}}\hat{\mathcal{E}}_{\mathrm{c}}^{\dagger}\},\end{aligned}\tag{A17}$$

$$\begin{aligned}\tilde{\sigma}_{14}=\frac{\mathrm{i}\xi_{32}}{D^{*}}\times\{&g_{\mathrm{c}}\hat{\mathcal{E}}_{\mathrm{c}}\,\mathrm{e}^{\mathrm{i}\boldsymbol{k}_{\mathrm{c}}\cdot\boldsymbol{r}}[\sigma_{11,33}\left(\frac{\xi_{21}^{*}}{\xi_{31}}+\frac{|\Omega_{\mathrm{P}_1\mathrm{P}2}|^2}{\xi_{31}\xi_{32}}\right)|\Omega_{\mathrm{P}_1}|^2\\&-(\frac{\xi_{21}^{*}|\Omega_{\mathrm{P}_2}|^2+\xi_{43}^{*}|\Omega_{\mathrm{P}_1}|^2}{\xi_{32}}+\xi_{21}^{*}\xi_{43}^{*})\sigma_{11,44}+|\Omega_{\mathrm{P}_2}|^2\\&\times\left(\frac{\xi_{43}^{*}}{\xi_{42}}-\frac{|\Omega_{\mathrm{P}_1\mathrm{P}2}|^2}{\xi_{42}\xi_{32}}\right)\sigma_{22,44}]+\Omega_{\mathrm{P}_1}\Omega_{\mathrm{P}_2}[\frac{\xi_{43}^{*}+\xi_{21}^{*}}{\xi_{32}}\sigma_{22,33}\\&+\left(\frac{\xi_{21}^{*}}{\xi_{42}^{*}}+\frac{|\Omega_{\mathrm{P}_1\mathrm{P}2}|^2}{\xi_{42}^{*}\xi_{32}}\right)\sigma_{22,44}\\&+\left(\frac{\xi_{43}^{*}}{\xi_{31}^{*}}-\frac{|\Omega_{\mathrm{P}_1\mathrm{P}2}|^2}{\xi_{31}^{*}\xi_{32}}\right)\sigma_{11,33}]\,\mathrm{e}^{\mathrm{i}\Delta\boldsymbol{k}_{\mathrm{c}}\cdot\boldsymbol{r}}g_{\mathrm{p}}\hat{\mathcal{E}}_{\mathrm{p}}^{\dagger}\},\end{aligned}\tag{A18}$$

where

$$\begin{aligned}D=&\,\xi_{41}\xi_{21}\xi_{43}\xi_{32}^{*}+(\xi_{41}\xi_{43}+\xi_{21}\xi_{32}^{*})|\Omega_{\mathrm{P}_1}|^2\\&+(\xi_{41}\xi_{21}+\xi_{43}\xi_{32}^{*})|\Omega_{\mathrm{P}_2}|^2+|\Omega_{\mathrm{P}_1\mathrm{P}2}|^4,\\|\Omega_{\mathrm{P}_1\mathrm{P}2}|^2=&\,|\Omega_{\mathrm{P}_1}|^2-|\Omega_{\mathrm{P}_2}|^2,\end{aligned}$$

$$\Delta \boldsymbol{k}_{\mathrm{p}} = \boldsymbol{k}_{\mathrm{P}_1} + \boldsymbol{k}_{\mathrm{P}_2} - \boldsymbol{k}_{\mathrm{c}},$$
$$\Delta \boldsymbol{k}_{\mathrm{c}} = \boldsymbol{k}_{\mathrm{P}_1} + \boldsymbol{k}_{\mathrm{P}_2} - \boldsymbol{k}_{\mathrm{p}}. \tag{A19}$$

Using the atomic operators to evaluate the linear and nonlinear components of the polarization at ω_{p} and ω_{c}, the polarization of the atomic medium at a particular frequency is given by $\hat{P}(\omega_{\mathrm{p}}) = Nd_{23}\tilde{\sigma}_{23} + \mathrm{H.c.}$ and $\hat{P}(\omega_{\mathrm{c}}) = Nd_{14}\tilde{\sigma}_{14} + \mathrm{H.c.}$ The polarization of the medium at frequency ω_{i} can be divided into two different terms: one is proportional to the field at frequency ω_{i} and the other is proportional to the field at frequency $\omega_{\mathrm{P}_1} + \omega_{\mathrm{P}_2} - \omega_{\mathrm{i}}$, such that

$$\hat{P}_{\mathrm{p}}(\omega_{\mathrm{p}}) = \varepsilon_0 \chi_{\mathrm{pp}}(\omega_{\mathrm{p}}) \hat{\mathcal{E}}_{\mathrm{p}} \mathrm{e}^{\mathrm{i}\boldsymbol{k}_{\mathrm{p}}\cdot\boldsymbol{r}} + \varepsilon_0 \chi_{\mathrm{pc}}(\omega_{\mathrm{p}}) \hat{\mathcal{E}}_{\mathrm{c}}^{\dagger} \mathrm{e}^{\mathrm{i}\Delta\boldsymbol{k}_{\mathrm{p}}\cdot\boldsymbol{r}} + \mathrm{H.c.}, \tag{A20}$$
$$\hat{P}_{\mathrm{c}}(\omega_{\mathrm{c}}) = \varepsilon_0 \chi_{\mathrm{cc}}(\omega_{\mathrm{c}}) \hat{\mathcal{E}}_{\mathrm{c}} \mathrm{e}^{\mathrm{i}\boldsymbol{k}_{\mathrm{c}}\cdot\boldsymbol{r}} + \varepsilon_0 \chi_{\mathrm{cp}}(\omega_{\mathrm{c}}) \hat{\mathcal{E}}_{\mathrm{p}}^{\dagger} \mathrm{e}^{\mathrm{i}\Delta\boldsymbol{k}_{\mathrm{c}}\cdot\boldsymbol{r}} + \mathrm{H.c.}, \tag{A21}$$

where the two coefficients χ_{pp} and χ_{cc} are given as follows:

$$\chi_{\mathrm{pp}} = \frac{\mathrm{i}N|d_{23}|^2\xi_{41}}{\varepsilon_0\hbar D}\Big[|\Omega_{\mathrm{P}_1}|^2\left(\frac{\xi_{43}}{\xi_{31}} + \frac{|\Omega_{\mathrm{P}_1\mathrm{P}2}|^2}{\xi_{31}\xi_{41}}\right)\sigma_{11,33} - \left(\frac{\xi_{43}|\Omega_{\mathrm{P}_2}|^2 + \xi_{21}|\Omega_{\mathrm{P}_1}|^2}{\xi_{41}} + \xi_{21}\xi_{43}\right)\sigma_{22,33} + |\Omega_{\mathrm{P}_2}|^2\left(\frac{\xi_{21}}{\xi_{42}} - \frac{|\Omega_{\mathrm{P}_1\mathrm{P}2}|^2}{\xi_{42}\xi_{41}}\right)\sigma_{22,44}\Big], \tag{A22}$$

$$\chi_{\mathrm{cc}} = \frac{\mathrm{i}N|d_{14}|^2\xi_{32}}{\varepsilon_0\hbar D^*}\Big[|\Omega_{\mathrm{P}_1}|^2\left(\frac{\xi_{21}^*}{\xi_{31}} + \frac{|\Omega_{\mathrm{P}_1\mathrm{P}2}|^2}{\xi_{31}\xi_{32}}\right)\sigma_{11,33} - \left(\frac{\xi_{21}^*|\Omega_{\mathrm{P}_2}|^2 + \xi_{43}^*|\Omega_{\mathrm{P}_1}|^2}{\xi_{32}} + \xi_{21}^*\xi_{43}^*\right)\sigma_{11,44} + |\Omega_{\mathrm{P}_2}|^2\left(\frac{\xi_{43}^*}{\xi_{42}} - \frac{|\Omega_{\mathrm{P}_1\mathrm{P}2}|^2}{\xi_{42}\xi_{32}}\right)\sigma_{22,44}\Big]. \tag{A23}$$

The two coefficients χ_{pc} and χ_{cp} are given by

$$\chi_{\mathrm{pc}} = \frac{\mathrm{i}Nd_{23}d_{14}\xi_{41}\Omega_{\mathrm{P}_1}\Omega_{\mathrm{P}_2}}{\varepsilon_0\hbar D}\Big[\frac{\xi_{21}+\xi_{43}}{\xi_{41}}\sigma_{11,44} + \left(\frac{\xi_{43}}{\xi_{42}^*} + \frac{|\Omega_{\mathrm{P}_1\mathrm{P}2}|^2}{\xi_{42}^*\xi_{41}}\right)\sigma_{22,44} + \left(\frac{\xi_{21}}{\xi_{31}^*} - \frac{|\Omega_{\mathrm{P}_1\mathrm{P}2}|^2}{\xi_{31}^*\xi_{41}}\right)\sigma_{11,33}\Big], \tag{A24}$$

$$\chi_{\mathrm{cp}} = \frac{\mathrm{i}Nd_{23}d_{14}\xi_{32}\Omega_{\mathrm{P}_1}\Omega_{\mathrm{P}_2}}{\varepsilon_0\hbar D^*}\Big[\frac{\xi_{43}^*+\xi_{21}^*}{\xi_{32}}\sigma_{22,33} + \left(\frac{\xi_{21}^*}{\xi_{42}^*} + \frac{|\Omega_{\mathrm{P}_1\mathrm{P}2}|^2}{\xi_{42}^*\xi_{32}}\right)\sigma_{22,44} + \left(\frac{\xi_{43}^*}{\xi_{31}^*} - \frac{|\Omega_{\mathrm{P}_1\mathrm{P}2}|^2}{\xi_{31}^*\xi_{32}}\right)\sigma_{11,33}\Big]. \tag{A25}$$

The two coefficients χ_{pp} and χ_{cc} describe the effective linear polarization processes for the probe and conjugate fields, respectively, and unlike the usual linear coefficients, they depend nonlinearly on the pump field. The other two coefficients χ_{pc} and χ_{cp} are responsible for the 4WM process.

Since the two pump fields have the same polarizations and frequencies, the two pump fields E_{P_1} and E_{P_2} also couple the transitions $|2\rangle \to |4\rangle$ and $|1\rangle \to |3\rangle$ with probabilities of $1/2$. Due to coupling another set of transitions with the same effective electric dipole, we just swap the Rabi frequencies Ω_{P_1} and Ω_{P_2} in the above 4 coefficients χ_{pp}, χ_{cc}, χ_{pc} and χ_{cp} to obtain a new set of transitions.

References

[1] Giovannetti V, Lloyd S and Maccone L 2004 *Science* **306** 1330
[2] Giovannetti V, Lloyd S and Maccone L 2011 *Nat. Photon.* **5** 222
[3] Degen C L, Reinhard F and Cappellaro P 2017 *Rev. Mod. Phys.* **89** 035002
[4] Abbott B P, Abbott R and Abbott T D *et al.* (LIGO Scientific Collaboration and Virgo Collaboration) 2016 *Phys. Rev. Lett.* **116** 061102
[5] Abbott B P, Abbott R and Abbott T D *et al.* (LIGO Scientific Collaboration and Virgo Collaboration) 2019 *Phys. Rev. X* **9** 031040
[6] Yurke B, McCall S L and Klauder J R 1986 *Phys. Rev. A* **33** 4033
[7] Jing J, Liu C, Zhou Z, Ou Z Y and Zhang W 2011 *Appl. Phys. Lett.* **99** 011110
[8] Hudelist F, Kong J, Liu C, Jing J, Ou Z Y and Zhang W 2014 *Nat. Commun.* **5** 3049
[9] Chen B, Qiu C, Chen S, Guo J, Chen L Q, Ou Z Y and Zhang W 2015 *Phys. Rev. Lett.* **115** 043602
[10] Qiu C, Chen S, Chen L Q, Chen B, Guo J, Ou Z Y and Zhang W 2016 *Optica* **3** 775
[11] Linnemann D, Strobel H, Muessel W, Schulz J, Lewis-Swan R J, Kheruntsyan K V and Oberthaler M K 2016 *Phys. Rev. Lett.* **117** 013001
[12] Lemieux S, Manceau M, Sharapova P R, Tikhonova O V, Boyd R W, Leuchs G and Chekhova M V 2016 *Phys. Rev. Lett.* **117** 183601
[13] Manceau M, Leuchs G, Khalili F and Chekhova M 2017 *Phys. Rev. Lett.* **119** 223604
[14] Anderson B E, Gupta P, Schmittberger B L, Horrom T, Hermann-Avigliano C, Jones K M and Lett P D 2017 *Optica* **4** 752
[15] Gupta P, Schmittberger B L, Anderson B E, Jones K M and Lett P D 2018 *Opt. Express* **26** 000391
[16] Du W, Jia J, Chen J F, Ou Z Y and Zhang W 2018 *Opt. Lett.* **43** 1051
[17] Plick W N, Dowling J P and Agarwal G S 2010 *New J. Phys.* **12** 083014
[18] Ou Z Y 2012 *Phys. Rev. A* **85** 023815
[19] Marino A M, Corzo Trejo N V and Lett P D 2012 *Phys. Rev. A* **86** 023844
[20] Li D, Yuan C H, Ou Z Y and Zhang W 2014 *New J. Phys.* **16** 073020
[21] Gabbrielli M, Pezzè L and Smerzi A 2015 *Phys. Rev. Lett.* **115** 163002
[22] Chen Z D, Yuan C H, Ma H M, Li D, Chen L Q, Ou Z Y and Zhang W 2016 *Opt. Express* **24** 17766
[23] Sparaciari C, Olivares S and Paris M G A 2016 *Phys. Rev. A* **93** 023810
[24] Li D, Gard B T, Gao Y, Yuan C H, Zhang W, Lee H and Dowling J P 2016 *Phys. Rev. A* **94** 063840
[25] Szigeti S S, Lewis-Swan R J and Haine S A 2017 *Phys. Rev. Lett.* **118** 150401
[26] Gong Q K, Hu X L, Li D, Yuan C H, Ou Z Y and Zhang W 2017 *Phys. Rev. A* **96** 033809
[27] Giese E, Lemieux S, Manceau M, Fickler R and Boyd R W 2017 *Phys. Rev. A* **96** 053863
[28] Hu X L, Li D, Chen L Q, Zhang K, Zhang W and Yuan C H 2018 *Phys. Rev. A* **98** 023803
[29] Wei C P, Hu X Y, Yu Y F and Zhang Z M 2016 *Chin. Phys. B* **25** 040601
[30] Gong Q K, Li D, Yuan C H, Ou Z Y and Zhang W P 2017 *Chin. Phys. B* **26** 094205
[31] Slusher R E, Hollberg L W, Yurke B, Mertz J C and Valley J F 1985 *Phys. Rev. Lett.* **55** 2409
[32] Schnabel R 2017 *Phys. Rep.* **684** 1
[33] Hemmer P R, Katz D P, Donoghue J, Cronin-Golomb M, Shariar M S and Kumar P 1995 *Opt. Lett.* **20** 982
[34] Lukin M D, Hemmer P R, Löffler M and Scully M O 1998 *Phys. Rev. Lett.* **81** 2675
[35] Zibrov A S, Lukin M D and Scully M O 1999 *Phys. Rev. Lett.* **83** 4049

[36] Balic V, Braje D A, Kolchin P, Yin G Y and Harris S E 2005 *Phys. Rev. Lett.* **94** 183601
[37] Kolchin P, Du S, Belthangady C, Yin G Y and Harris S E 2006 *Phys. Rev. Lett.* **97** 113602
[38] Thompson J K, Simon J, Loh H and Vuletic V 2006 *Science* **313** 74
[39] van der Wal C H, Eisaman M D, André A, Walsworth R L, Phillips D F, Zibrov A S and Lukin M D 2003 *Science* **301** 196
[40] McCormick C F, Boyer V, Arimondo E and Lett P D 2007 *Opt. Lett.* **32** 178
[41] McCormick C F, Marino A M, Boyer V and Lett P D 2008 *Phys. Rev. A.* **78** 043816
[42] Zhang Z, Wen F, Che J, Zhang D, Li C, Zhang Y and Xiao M 2015 *Sci. Rep.* **5** 15058
[43] Zhang D, Li C, Zhang Z, Zhang Y, Zhang Y and Xiao M 2017 *Phys. Rev. A* **96** 043847
[44] Liu C, Jing J, Zhou Z, Pooser R C, Hudelist F, Zhou L and Zhang W 2011 *Opt. Lett.* **36** 2979
[45] Ma R, Liu W, Qin Z, Su X, Jia X, Zhang J and Gao J 2018 *Opt. Lett.* **43** 1243
[46] Wu M C, Schmittberger B L, Brewer N R, Speirs R W, Jones K M and Lett P D 2019 *Opt. Express* **27** 4769
[47] Boyer V, Marino A M and Lett P D 2008 *Phys. Rev. Lett.* **100** 143601
[48] Boyer V, Marino A M, Pooser R C and Lett P D 2008 *Science* **321** 544
[49] Qin Z, Cao L, Wang H, Marino A M, Zhang W and Jing J 2014 *Phys. Rev. Lett.* **113** 023602
[50] Qin Z, Cao L and Jing J 2015 *Appl. Phys. Lett.* **106** 211104
[51] Du W, Kong J, Jia J, Ming S, Yuan C H, Chen J F, Ou Z Y, Mitchell M W, Zhang W arXiv:2004.14266
[52] Corzo N V, Marino A M, Jones K M and Lett P D 2012 *Phys. Rev. Lett.* **109** 043602
[53] Embrey C S, Turnbull M T, Petrov P G and Boyer V 2015 *Phys. Rev. X* **5** 031004
[54] Wang L H, Fabre C and Jing J 2017 *Phys. Rev. A* **95** 051802
[55] Cao L, Qi J, Du J and Jing J 2017 *Phys. Rev. A* **95** 023803
[56] Jia J, Du W, Chen J F, Yuan C H , Ou Z Y and Zhang W 2017 *Opt. Lett.* **42** 4024
[57] Turnbull M T, Petrov P G, Embrey C S, Marino A M and Boyer V 2013 *Phys. Rev. A* **88** 033845
[58] Corzo N, Marino A M, Jones K M and Lett P D 2011 *Opt. Express* **19** 21358
[59] Jasperse M, Turner L D and Scholten R E 2011 *Opt. Express* **19** 3765
[60] Knutson E M, Swaim J D, Wyllie S and Glasser R T 2018 *Phys. Rev. A* **98** 013828
[61] Davis W V, Kauranen M, Nagasako E M, Gehr R J, Gaeta A L and Boyd R W 1995 *Phys. Rev. A* **51** 4152
[62] Steck D A https://steck.us/alkalidata/
[63] Boyer V, McCormick C F, Arimondo E and Lett P D 2007 *Phys. Rev. Lett.* **99** 143601
[64] Glasser R T, Vogl Ulrich and Lett Paul D 2012 *Phys. Rev. Lett.* **108** 173902